6.3 Electron Lattice Design and Beam Stability

This section of the report deals with the design of the electron lattice and the dynamical stability of the electron beam. Higher luminosity requires smaller beam sizes at the interaction points (IPs). Reducing both the equilibrium emittance and the beam envelope functions (β_x^*, β_y^*) at the IPs lowers the electron beam size. However this reduction in beam sizes also increases the electromagnetic force between the beams which can cause beam losses and thereby limits the extent to which luminosity can be increased. Constraints from this beam-beam force and the forces from the nonlinear sextupole fields have guided the new design of the electron lattice.

The equilibrium emittance of the electrons can be reduced with stronger focusing in the FODO cells in the arcs while the β^* can be lowered by increasing the integrated quadrupole strengths in the interaction regions and moving these quadrupoles closer to the IP. The stronger focusing in the interaction regions increases the chromaticity of the electron lattice and hence requires stronger sextupoles to correct the chromaticity. In turn the stronger non-linear forces on the beam reduce the stable phase space area (the "dynamic aperture") available to the beam. It is essential that the new design of the optics in the interaction regions be such that while squeezing the beam down to a smaller spot size at the interaction points, a sufficiently large dynamic aperture is preserved to avoid significant beam losses during colliding beam operation. A number of lattices were studied to optimize the design and the results of these studies are presented here. We examine the issues in turn: a) design of the focusing in the arcs, b) correction of the chromaticity by sextupoles, and c) the resulting dynamic aperture for each of these lattices.

6.3.1 Electron Lattice

The electron lattice is composed of four quadrants: North, East, South and the West with the North and South quadrants being identical. Each quadrant can be further split into two identical octants. Each octant consists of an arc with 18 FODO cells, a matching section 7 FODO cells long, a spin rotator section (in the North, East, South), an RF section, and then a straight section up to the interaction point. The optics changes in the lattice are the following:

- Increase of the focusing in the FODO cells.
- Pairs of spin rotators in the North and South straight sections.
- Redesign of the North and the South interaction regions with the two beams separated earlier (closer to the IP) and stronger focusing with quadrupoles moved closer to the IP.

Phase advances in the FODO cells

The electron equilibrium emittance is obtained as a balance between the damping of betatron oscillations due to the synchrotron radiation and excitation due to photon emission. The emittance has to be reduced from its present values to reduce the beam size at the IPs. This can be done by increasing the focusing in the FODO cells. For a machine with only FODO cells, the equilibrium emittance scales with the horizontal phase advance μ_x^C per FODO cell as [1]

$$\epsilon_x(\mu_x^C) \sim \frac{1 - \frac{3}{4}\sin^2(\mu_x^C/2) + \frac{1}{60}\sin^4(\mu_x^C/2)}{\sin^2(\mu_x^C/2)\sin\mu_x^C} \tag{7}$$

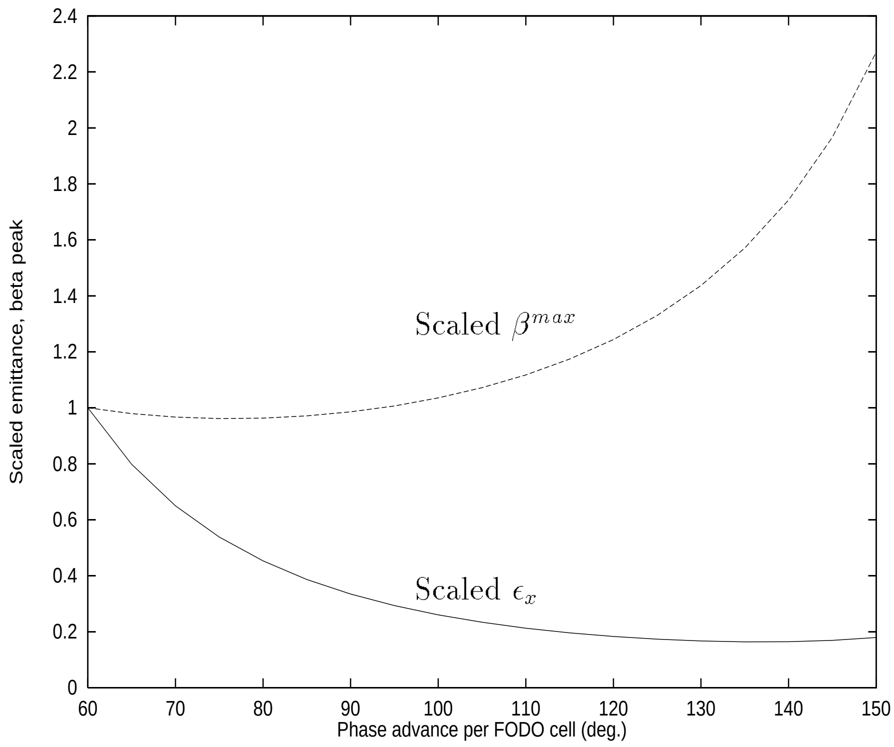

Figure 19: Scaled equilibrium emittance and maximum of the beta function as a function of the phase advance in a FODO cell.

The maximum of the β function in a cell is given by

$$\beta^{max} = L_C \left[\frac{1 + \sin(\mu^C/2)}{\sin \mu^C} \right] \tag{8}$$

where $L_C = 23.51$m is the length of a FODO cell in HERA-e. Figure 19 shows the change in the emittance and β^{max} (scaled to the values at $\mu^C = 60$ degrees) with increasing phase advance.

The equilibrium emittance decreases monotonically as the phase advance is increased reaching a minimum at a phase advance of $\mu^C = 135$ degrees before increasing again. However β^{max} in the cell reaches its minimum at $\mu^C = 73.6$ degrees and at 135 degrees is already at 1.6 times its value at $\mu^C = 60$ degrees. Since the dynamic aperture roughly scales with the inverse of the β peak, it is advisable to keep this value low. A compromise choice for the horizontal phase advance which reduces the equilibrium emittance sufficiently is μ^C=90 degrees. The above scaling relation for FODO cells predicts that at 90 degrees, the equilibrium emittance will be reduced to 14nm from the present value of about 41nm. In practice, the emittance will be higher because the ring has regions with high dispersion and bends adjacent to all four straight sections . At this value of $\mu^C = 90$degrees, β^{max} is slightly lower than with 60 degrees. This also has the advantage that only two sextupole families are required in the horizontal plane for nonlinear chromaticity correction. The vertical beam size is determined by the emittance coupling ratio $\kappa = \epsilon_y/\epsilon_x$ and is independent of the vertical phase advance. The optimal choice of the vertical phase advance is therefore one which minimizes the chromaticity of the whole lattice and hence reduces the required sextupole strengths. We will examine this in the section on chromaticity correction.

Region	East, South, North	West
Matching Section Quadrupoles	QK30, QK31, ... QK43	QK62, QK63, ... QK75
RF section	QL14, QL15, ... QL24	QL47, QL48, ... QL52
Spin Rotator	QC25, QC26, ... QC29	—

Table 6: Quadrupoles in the different sections between an arc and inner straight sections.

Matching Section

Each matching section which has the length of 7 FODO cells has a FODO cell like structure with regular dipoles in between quadrupoles. The quadrupoles however have variable gradients and are used to match the optics functions from the straight sections into the arcs.

The dispersion function reaches its peak values in the matching sections so photon emission in these regions contributes more to the growth of the equilibrium emittance per unit length than in any other region. The matching quadrupoles must therefore be used to both match into the arcs and minimize the peak dispersion in these regions.

Spin Rotator section

Each spin rotator has seven horizontal bend dipoles and 4 vertical bend dipoles with zero net vertical bend. The addition of the spin rotators in the North and the South is new in this lattice. One of the spin matching constraints requires that

$$\tan \Delta\mu(s) = -\alpha(s) \tag{9}$$

where $\Delta\mu(s)$ is the phase advance from the IP to the point in question and α is the Twiss function at this location. This constraint has to be satisfied in both planes. This can be met by providing a waist (where $\alpha_x = 0 = \alpha_y$) in the middle of the spin rotator and setting the phase advance from the IP to the waist equal to an integer multiple of π. The same spin matching condition also puts a constraint on the slope of the dispersion function at the entrance of the spin rotator. The sum of this slope and the bend angle in the rotator must equal the total bend angle (= bend angle in a FODO cell) between the IP and the entrance to the matching section.

RF section

The RF section houses the cavities and 5 periods of alternately focusing and defocusing quadrupoles. The total of 82 cavities are distributed as: 26 in the East straight, 24 each in the South and North straights and 8 cavities in the West utility. Dispersion in this section must be minimized in order to avoid exciting synchro-betatron resonances.

Putting it all together

The design of the inner interaction region has been described in an earlier section. The Twiss functions from this region are matched into the regular FODO cells using the above mentioned quadrupoles and satisfying the necessary constraints also mentioned above. Figures 20 to 22 show the β functions and the horizontal dispersion through a section from the beginning of one matching section to the end of the next matching section with the interaction region in the center in the REV 1 design. In the current design of the lattice now operational, the maximum β functions in the RF section are about 90m in both planes. This is still true in the REV 1 design. However the vertical β peak in QC29 is about 200m in the REV1 design. It remains to be checked that this is not an aperture restriction. Table 6 shows the quadrupoles in the different regions of the lattice.

Figures 23 to 25 show the optics functions through the complete ring, starting from the East IP.

6.3.2 Chromaticity Correction

In this section we will discuss the following in order:

- Choice of the optimal phase advances in the FODO cells to minimize the total linear chromaticity.
- Comparison of the chromaticity correction for the different lattices studied.
- Out of these studies evolved a choice for the optimal phase advances. The focusing in the interaction regions was subsequently increased following a change in parameters. This lattice (named REV1) with optimal phase advances in the FODO cells, stronger focusing in the interaction regions with normal conducting magnets is the baseline design lattice.

The total linear chromaticity of the lattice can be conveniently split into two parts: one coming from all the FODO cells and the other from the straight sections. In the thin lens approximation of quadrupoles in a FODO cell, the linear chromaticity of each cell is given by

$$\xi^C = -\frac{1}{\pi}\tan\frac{\phi_c}{2} \tag{10}$$

where ϕ_c is the phase advance through the cell. This is usually a good approximation for the chromaticities in each plane when the phase advances are the same in both planes. Thus it predicts that the absolute value of the chromaticity increases monotonically as the phase advance increases from 0 to 90 degrees. However when the phase advances in the two planes are not equal, the exact chromaticity differs significantly from the value predicted by the above formula. Figure 26 shows the chromaticity in each plane when the horizontal phase is kept constant at 90 degrees and the vertical phase varied.

This shows that the horizontal chromaticity increases in absolute value as the vertical phase advance is increased. The absolute vertical chromaticity *decreases* as the phase advance increases from 30 degrees, has a minimum at a phase advance of 40 degrees before increasing monotonically. Table 7 shows the chromaticity contribution $\xi_x^{Arcs}, \xi_y^{Arcs}$ from 200 FODO cells at 3 different values of the vertical phase advance. The vertical phase advances chosen are those for which the number of sextupole families required in the vertical plane will be less than 5.

This table shows that there is a relatively large increase in vertical chromaticity when the vertical phase advance is set to 90 degrees. It is better to lower the phase advance to 60 or even 45 degrees. The difference in chromaticities between these two options is relatively small. However the number of sextupole families per plane needed is 3 with 60 degrees and 4 when

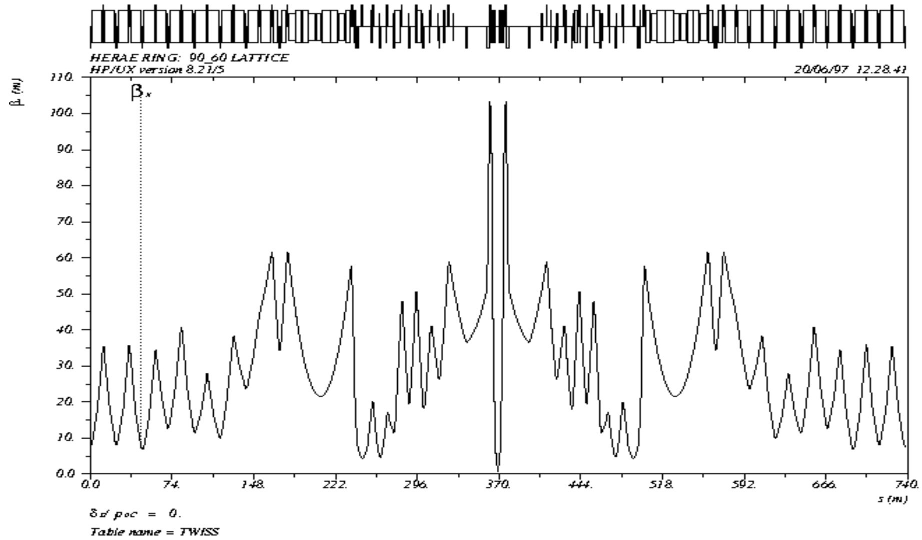

Figure 20: The horizontal beta function through a section including the inner IR, RF sections and matching sections in the REV1 design.

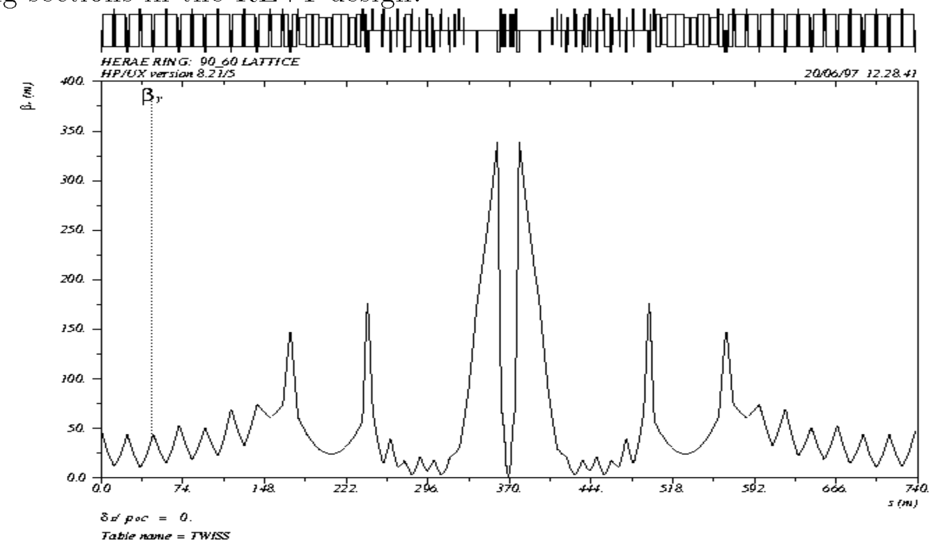

Figure 21: The vertical beta function through a section including the inner IR, RF sections and matching sections in the REV1 design.

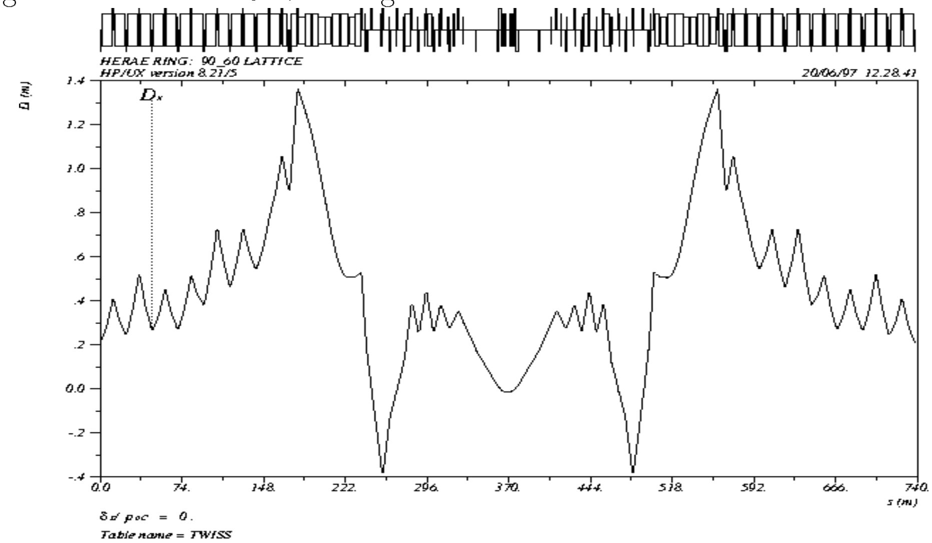

Figure 22: The horizontal dispersion function through a section including the inner IR, RF sections and matching sections in the REV1 design.

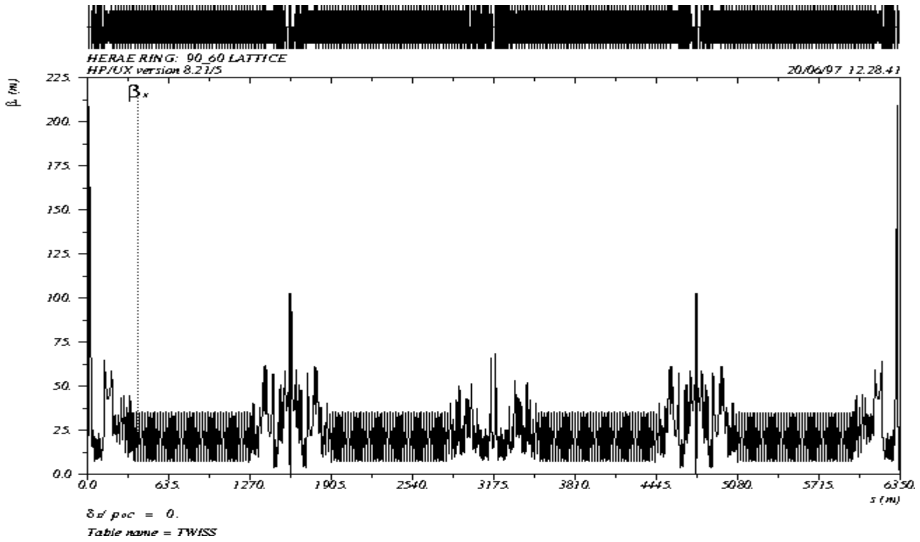

Figure 23: The horizontal beta function through the complete ring in the REV1 design.

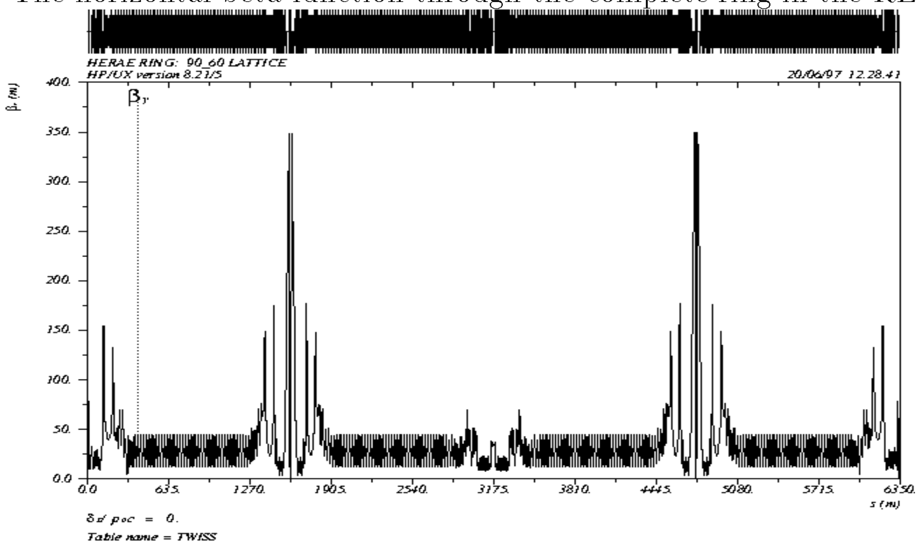

Figure 24: The vertical beta function through the complete ring in the REV1 design.

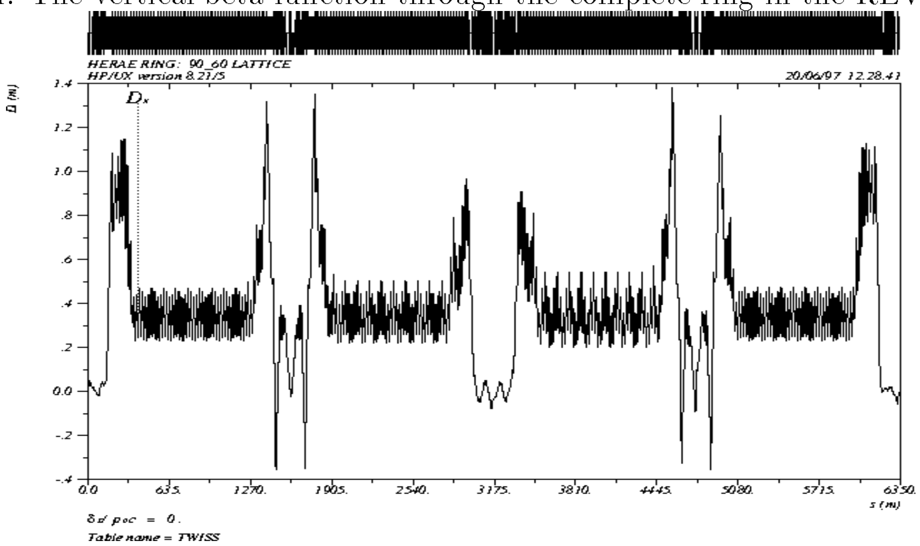

Figure 25: The horizontal dispersion function through the complete ring in the REV1 design.

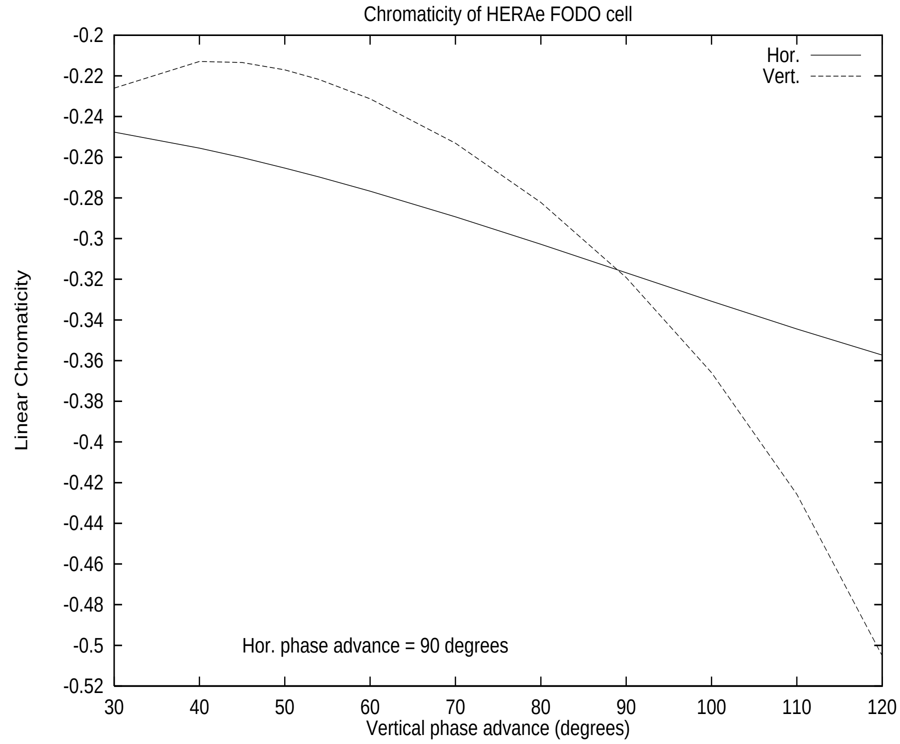

Figure 26: Horizontal and vertical chromaticities of the HERA-e FODO cell as a function of the vertical phase advance per cell calculated exactly. The horizontal phase is constant at 90 degrees.

Phase advance per cell (μ_x^C, μ_y^C) degrees	Chromaticity of 200 FODO cells (ξ_x^{Arcs}, ξ_y^{Arcs})
(90, 45)	(-52.0, -42.7)
(90, 60)	(-55.3, -46.2)
(90, 90)	(-63.3, -63.8)

Table 7: Chromaticity of 200 FODO cells with the horizontal phase advance per cell μ_x^C = 90degrees and different vertical phase advances μ_y^C

$(\mu_x^C,\, \mu_y^C)$ degrees	S_F [m^{-3}]	S_D [m^{-3}]
(90, 45)	1.53	-1.05
(90, 60)	1.49	-1.18
(90, 90)	1.39	-1.40

Table 8: Sextupole strengths required for correcting the linear chromaticity with different choices of the vertical phase advance per FODO cell and the REV1 design for the IRs

the phase advance is 45 degrees. If we choose 60 degrees for the vertical phase advance, then the linear chromaticity is near the absolute minimum and the number of sextupole families is also small.

Sextupoles are placed in the arc cells where the dispersion is non-zero. In the HERA-e lattice there are some cells in the centers of the arcs which do not have sextupoles in them. Consequently the numbers of cells with sextupoles N_S is less than 200. The strengths (in units of m^{-3}) of the linear chromaticity correcting sextupoles can be found from the following expressions

$$
\begin{aligned}
S_F &= \frac{4\pi}{L_F N_S D_x^{max}(\beta_x^{max}\beta_y^{max} - \beta_x^{min}\beta_y^{min})}\left\{[C_x - \xi_x^{latt}]\beta_y^{max} + [C_y - \xi_y^{latt}]\beta_x^{min}\right\} && (11)\\
S_D &= -\frac{4\pi}{L_D N_S D_x^{min}(\beta_x^{max}\beta_y^{max} - \beta_x^{min}\beta_y^{min})}\left\{[C_x - \xi_x^{latt}]\beta_y^{min} + [C_y - \xi_y^{latt}]\beta_x^{max}\right\} && (12)\\
\xi_x^{latt} &= \xi_x^{Arcs} + \xi_x^{str} && (13)\\
\xi_y^{latt} &= \xi_y^{Arcs} + \xi_y^{str} && (14)
\end{aligned}
$$

L_F, L_D are the lengths of the S_F, S_D sextupoles respectively. The minimum and maximum Twiss functions β_x, β_y, D_x refer to the extreme values in a FODO cell. C_x, C_y are the corrected values of the linear chromaticity typically set to +1 in both planes. ξ_x^{str}, ξ_y^{str} are the chromaticities of the straight sections and their values are dominated by the contributions from the North and South interaction regions. With $L_F = 0.28$m, $L_D = 0.62$m, $N_S = 192$ and assuming the REV1 design for the interaction regions, we obtain the values for the sextupole strengths shown in Table 8.

In the present HERA-e ring with 60 degree phase advance in both planes, sextupoles are grouped into 3 families in each plane. The families are the same in the North and the South quadrants but different in the East and West quadrants. The absolute minimum and maximum sextupole strengths are (0.41, 0.88) M^{-3} respectively. The stronger focusing in the arcs and in the interaction regions in the upgraded optics will require the sextupole strengths to be nearly doubled.

Correcting the non-linear chromaticity

The tune shift ΔQ due to chromatic errors can be written as a power series in the relative momentum deviation $\delta = \Delta p/p_0$ as

$$\Delta Q = \xi_1\delta + \xi_2\delta^2 + \ldots \qquad (15)$$

The upgraded interaction region is a source of large linear and non-linear chromaticity. The linear chromaticity generated by the quadrupoles is

$$\xi_1 = -\frac{1}{4\pi}\int_0^C \beta_0(s)K(s)ds \tag{16}$$

where $\beta_0(s)$ is the nominal beta function and $K(s)$ the gradient in units of m^{-2}. The higher order chromaticities, unlike ξ_1, depend on the phase relationships between the chromatic sources. The second order chromaticity, for example, is given compactly by [2]

$$\xi_2 = -\frac{1}{8\pi}\int_0^C K(s)\Delta\beta_1(s)ds - \xi_1 \tag{17}$$

where $\Delta\beta_1(s)$ is the first order chromatic beta wave,

$$\Delta\beta_1(s) = \frac{\beta_0(s)}{2\sin 2\pi Q_0}\int_s^{s+C} K(s')\beta_0(s')\cos[2\pi Q_0 - 2|\psi_0(s') - \psi_0(s)|]ds' \tag{18}$$

$\psi_0(s)$ is the phase advance from a reference point to point s. These expressions show that the second order chromaticity (and indeed higher order ones) depend on the global tune Q_0 and that the beta wave propagates at twice the betatron frequency. As a function of the tune, the second (and higher order) chromaticities are a minimum around $Q_0 = 0.25$. The interaction region quadrupoles with their large gradients and high beta functions are the primary sources of the chromatic beta wave propagating in the ring. This beta wave must be damped in order to reduce the second and higher order chromaticities.

The sextupoles introduced to correct the linear chromaticity must also reduce the nonlinear chromaticity and do it so as not to introduce large nonlinear effects in the transverse planes (or higher order geometric aberrations). One way of doing this is to place sextupoles in modules with phase advances of an integer multiple of 2π. If the number of cells within a module is either two or greater than three, then the following resonance driving terms:

$$\sum_k \beta_{x,k}^{3/2}\bar{S}_k e^{i\psi_{x,k}}, \qquad \sum_k \beta_{x,k}^{1/2}\beta_{y,k}\bar{S}_k e^{i\psi_{x,k}}, \qquad \sum_k \beta_{x,k}^{3/2}\bar{S}_k e^{3i\psi_{x,k}}, \qquad \sum_k \beta_{x,k}^{1/2}\beta_{y,k}\bar{S}_k e^{i[\psi_{x,k}\pm 2\psi_{y,k}]} \tag{19}$$

sum to zero [3] where

$$\bar{S} = \frac{1}{2(B\rho)}\int \frac{\partial^2 B_y}{\partial x^2}ds \simeq \frac{1}{2(B\rho)}B_y''l \tag{20}$$

is the integrated sextupole strength. This implies that all second order geometric aberrations vanish. Higher order aberrations can be reduced by placing sextupoles in families with members of a family π apart in phase [3]. Sextupoles produce kicks that are even order in the coordinates,

$$\Delta x' = -\bar{S}[(x + D_x\delta)^2 - y^2] \tag{21}$$

$$\Delta y' = -2\bar{S}[x + D_x\delta]y \tag{22}$$

For an on-momentum particle ($\delta = 0$), the kicks due to two sextupoles separated by an -I transformation are equal and opposite. Since the positions and slopes at the second sextupole are the negative of those at the first sextupole, there is no effect on these particles outside the region of these sextupoles. For these particles, all nonlinear geometric aberrations cancel provided there is an even number of sextupoles per family. The cancellation for off-momentum particles is not as good because the phase advance between the sextupoles is different from

k	l	μ_C (degrees)
0	2, 3, 4, 6, ...	90, 60, 45, 30, ...
1	4, 8, ...	135, 67.5, ...
2	8, 12, ...	112.5, 75, ..

Table 9: Possible choices of phase advance per cell with sextupole families π apart.

π and the transverse displacement depends on the horizontal dispersion. Furthermore in an interleaved sextupole scheme where there are other sextupoles between the -I pair, there are cross terms due to the interleaving sextupoles and the cancellation at the end of each -I pair is not exact even for on-momentum particles. Nevertheless, there is an approximate cancellation of higher order chromatic and non-linear effects for all particles in the beam and it can often be sufficient to yield an acceptable dynamic aperture across the full momentum range.

Requiring that sextupoles in a family be π apart constrains the phase advance per cell to be

$$\mu_C = \frac{(2k+1)}{l}\pi \tag{23}$$

where k, l are integers and the total number of cells with sextupoles N_S is an even integer times l. Some of the possible choices with $N_S = 192$ and requiring that the phase advance per cell does not exceed 135 degrees (the phase at which the equilibrium emittance attains its minimum value),are shown in Table 9

The choice of 90 degrees for the horizontal phase advance gives both a smaller equilibrium emittance and smaller nonlinear geometric aberrations. A seeming drawback to this choice is that the chromatic beta wave generated by the sextupoles in one plane are π apart in phase. Hence the chromatic beta wave generated by the interaction region quadrupoles can only be partially cancelled (the sine-like component can be removed but not the cosine-like component) unless the phase advance from the IP to the nearest sextupole is chosen to be 90 degrees. One way out of this constraint on the phase advance in the interaction region is to allow the two interaction regions in the ring to generate oppositely phased chromatic beta waves so that they cancel each other. This can be done with a phase advance of 90 degrees (modulo 2π) between the two IPs. During operations it may happen that the optics needs to be changed for whatever reason by a resetting of the main arc quadrupoles and thus destroying the optimum phase advance between the IPs. In that case, since there are at present no constraints on the phase advance through the West straight section, the quadrupoles in this section can be retuned to have the proper phase advance between the IPs.

In an earlier HERA report [4], phase advances were chosen to make only the second order aberrations vanish. Thus sextupoles are placed in blocks of N FODO cells with phase advances per cell

$$\mu_C = \frac{M}{N} 2\pi \tag{24}$$

with M, N being integers. With 25 cells per octant, one possible choice of phase advance is $\mu_C = (6/25) \times 2\pi = 86.4$ degrees. This choice of phase advance is large enough to get the required low emittance and also does away with special phase advances in different sections of the ring. However it does not reduce the higher order (larger than second) geometric aberrations.

Lattice	Phase Advance (degrees) (Horizontal, Vertical)	No. of sextupole families (Horizontal, Vertical)
CURRENT	(60, 60)	(3, 3)
I	(90, 90)	(2, 2)
II (REV 0)	(90, 60)	(2, 3)
III	(86.4, 90)	(5, 3)
REV 1	(90, 60)	(2, 3)

Table 10: Phase advances and sextupole families for the cases studied

We investigated the chromaticity correction and the resulting dynamic aperture for three different choices of phase advance in the FODO cells. Table 10 shows the phase advances and the number of sextupole families required in each plane. The optics in the North and South IRs was the same in all of these lattices. Table 11 shows the main optics parameters for these lattices. For comparison, the parameters of the lattice now in operation (labelled `CURRENT`) are also shown. The equilibrium vertical emittance ϵ_y corresponds to the values obtained from the linear optics programs with coupling being generated solely by the vertical bend dipoles in the spin rotators. The coupling in the machine is considerably higher with a correspondingly larger value of ϵ_y.

The nonlinear chromaticity correction was done using the module HARMON in MAD [6]. This program can be used to correct second and third order chromaticities with a distribution of sextupoles and also reduce the geometric aberrations by lowering the tune shift with amplitude. The chromaticity correction can be done a variety of ways by placing different weights on the second and third order chromaticities. To compare the quality of the three lattices shown in Table 10 in a consistent fashion, only the second order chromaticity was set to zero. HARMON calculates the following nonlinear parameters: the chromaticities

$$Q_x'' \equiv \frac{d^2Q_x}{d\delta^2}, \qquad Q_y'' \equiv \frac{d^2Q_y}{d\delta^2}, \qquad Q_x''' \equiv \frac{d^3Q_x}{d\delta^3}, \qquad Q_y''' \equiv \frac{d^3Q_y}{d\delta^3}$$

and also the derivative of the tunes with emittance evaluated at zero amplitude, $dQ_x/d\epsilon_x$, $dQ_y/d\epsilon_y$, $dQ_y/d\epsilon_x$. Table 12 shows how these nonlinear figures of merit calculated after correction compare for the three lattices.

The figures of merit in Table 12 and Figures 27 and 28 show that the chromaticity correction for the (90, 90) lattice is an order of magnitude better than for the lattices II and III, but at the expense of stronger sextupoles. Consequently the detuning with amplitude is about two orders of magnitude larger in the vertical plane for this lattice than for the others. This can be expected to have an adverse effect on the dynamic aperture which will be seen in the next section. Comparison of the (90,60) and (86.4,60) lattices shows that the tune corrections are nearly the same while the chromatic variation of β^* in the (86.4,60) lattice is much worse. $dQ_x/d\epsilon_x$ is more than an order of magnitude smaller for the (90,60) lattice. This lattice also has the nice feature that $dQ_y/d\epsilon_y$ and $dQ_y/d\epsilon_x$ have opposite signs so that at large transverse amplitudes, the vertical tune will stay nearly constant. By contrast, $dQ_y/d\epsilon_y$ and $dQ_y/d\epsilon_x$ are both negative for the (86.4,60) lattice so that it is possible for a tune above resonance at small

Lattice	Equilib. Emitt. (ϵ_x, ϵ_y) [nm]	β^*[m] at IP (β_x^*, β_y^*)	β^{max}[m] $(\beta_x^{max}, \beta_y^{max})$	D^{max}[m] (D_x^{max}, D_y^{max})	Chromaticity (Q'_x, Q'_y)
CURRENT	(41.37, 0.27)	(1.0, 1.0)	(219.2, 164.4)	(2.17, 0.21)	(-66.1, -62.4)
I	(22.7, 0.62)	(0.83, 0.35)	(217.6,342.2)	(1.62,0.22)	(-81.7, -98.2)
II (REV 0)	(18.9, 0.78)	(0.83, 0.35)	(212.7,342.2)	(1.61,0.22)	(-76.2, -84.1)
III	(23.4, 0.55)	(0.83, 0.35)	(204.8,345.9)	(1.33, 0.22)	(-75.1, -84.5)
REV 1	(21.2, 0.72)	(0.63, 0.26)	(211.6, 347.7)	(1.15, 0.22)	(-79.7, -87.2)

Table 11: Main optics parameters for the lattices studied. The values of β^* are those at the North and South IPs.

Lattice	(Q''_x, Q''_y)	(Q'''_x, Q'''_y)
CURRENT	(-7.27×10^1, -2.17×10^1)	(9.76×10^3, 8.97×10^2)
I	(1.15×10^{-4}, -1.46×10^{-4})	(2.91×10^3, 5.14×10^3)
II (REV 0)	(-5.24×10^{-6}, -7.12×10^{-7})	(2.47×10^3, 5.86×10^4
III	(-3.89×10^{-5}, 5.96×10^{-4})	(4.18×10^3, 4.68×10^4)
REV 1	(-7.70, 5.81×10^{-1})	(1.74×10^4, -3.33×10^2)

Lattice	$dQ_x/d\epsilon_x$ [m^{-1}]	$dQ_y/d\epsilon_y$ [m^{-1}]	$dQ_y/d\epsilon_x$ [m^{-1}]
CURRENT	-1.13×10^3	-8.74×10^2	-2.80×10^3
I	-4.03×10^2	1.80×10^5	-3.73×10^5
II (REV 0)	8.23×10^1	6.21×10^3	-9.50×10^3
III	1.53×10^3	-2.93×10^3	-4.98×10^4
REV 1	-1.12×10^3	3.55×10^2	-3.89×10^3

Table 12: Nonlinear figures of merit for the lattices with higher order chromaticity correction

amplitudes to be pulled into the resonance at large amplitudes. These observations will be compared against tracking results in the next section.

Finally another lattice was studied. The IR optics was changed to one with stronger focusing so that the electron beam with an equilibrium emittance of 22 nm could be matched to the proton beam at the IPs. This lattice has phase advances of (90, 60) degrees and is designated `REV 1`. Table 11 shows the main optics parameters. Nonlinear chromaticity correction was done to minimize both the second and third order chromaticities. Table 12 shows the nonlinear figures of merit. Figures 29 and 30 show the chromatic behaviour of the tunes and β^* at the South IP as a function of the momentum deviation δ.

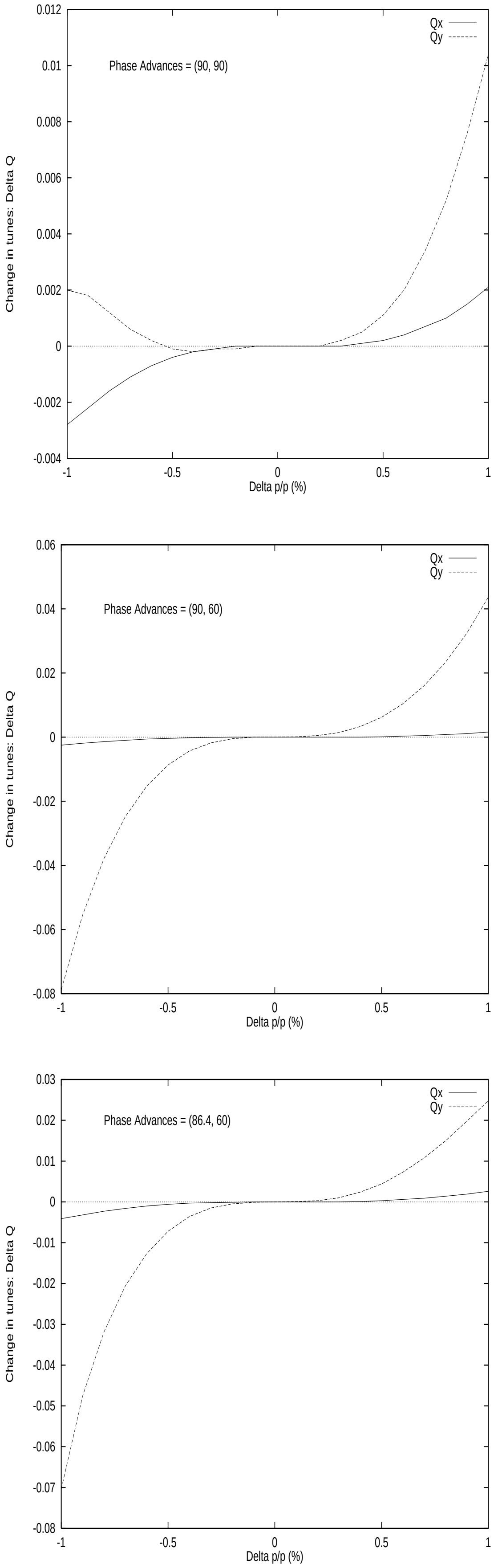

Figure 27: Tune shift vs δ for the different lattices

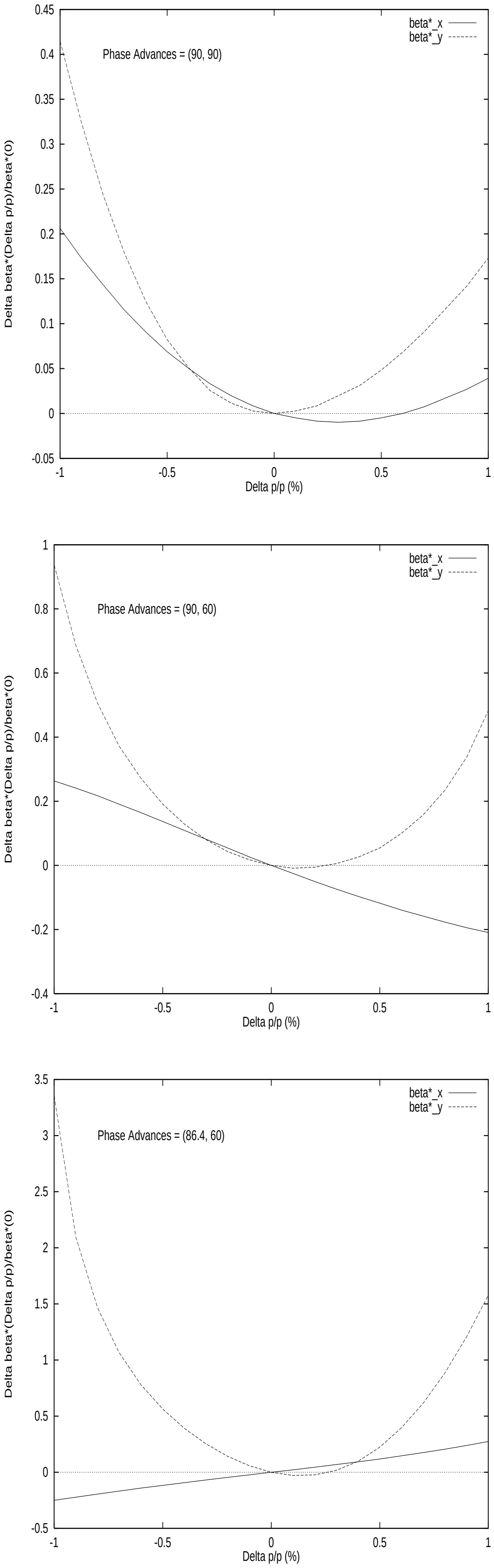

Figure 28: β^* at the South IP vs δ for the different lattices

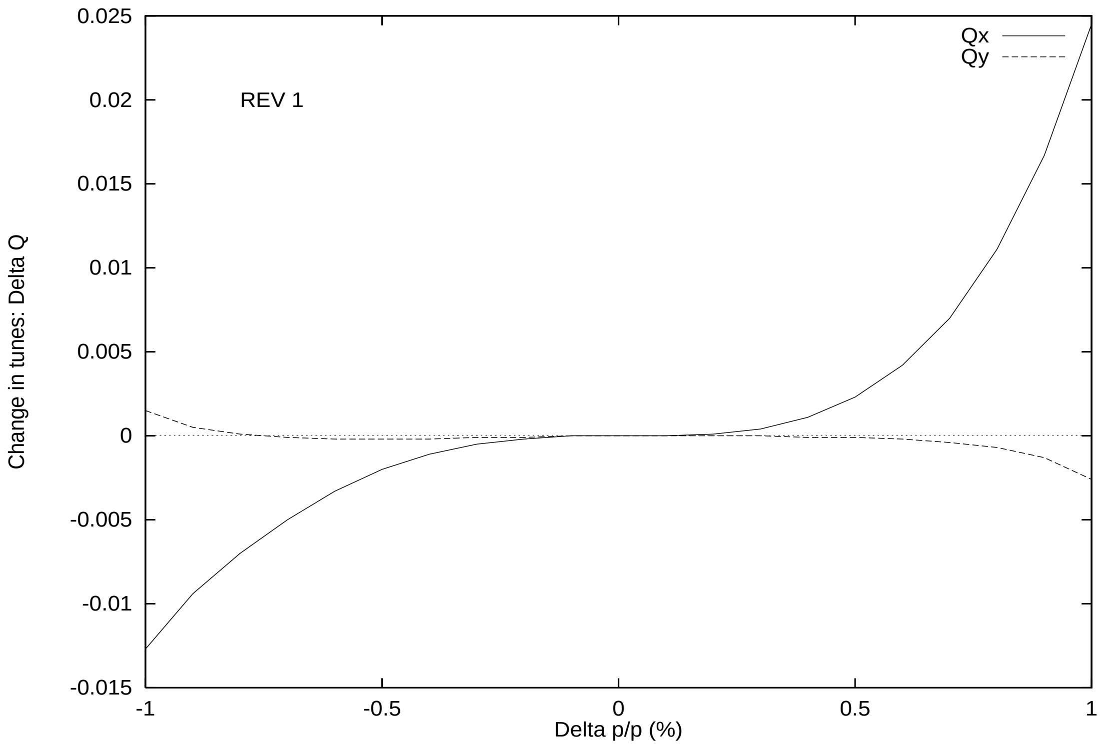

Figure 29: Tune shift vs δ for the REV 1 lattice

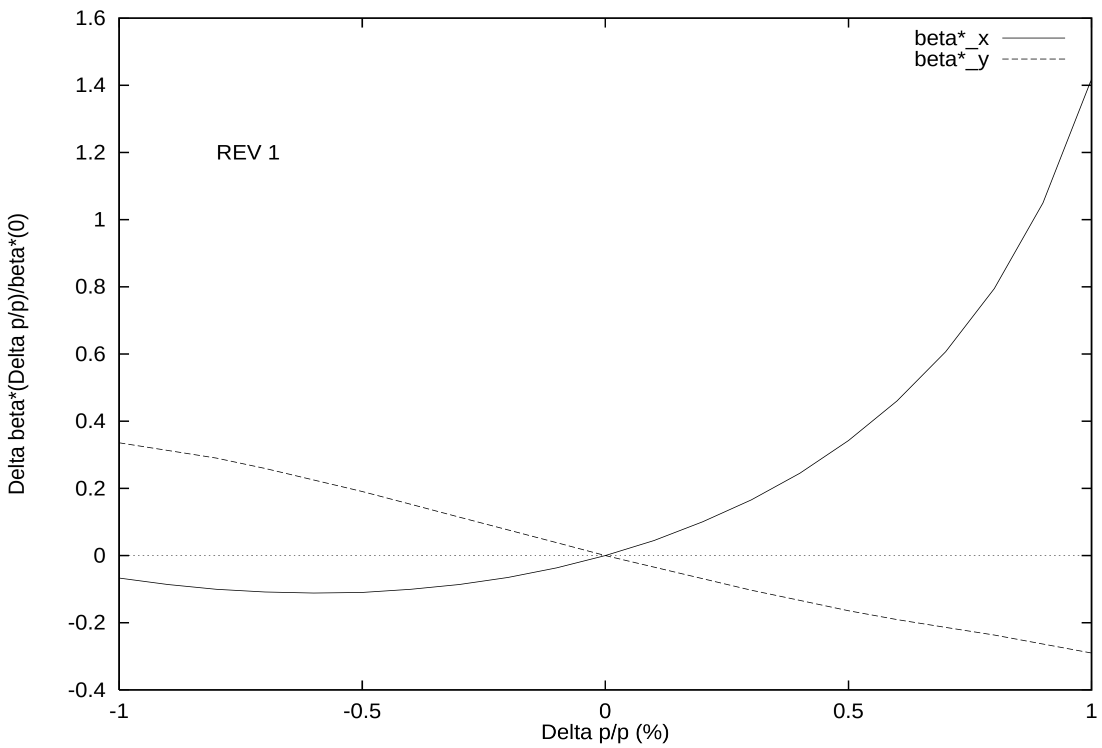

Figure 30: β^* at the South IP vs δ for the REV 1 lattice

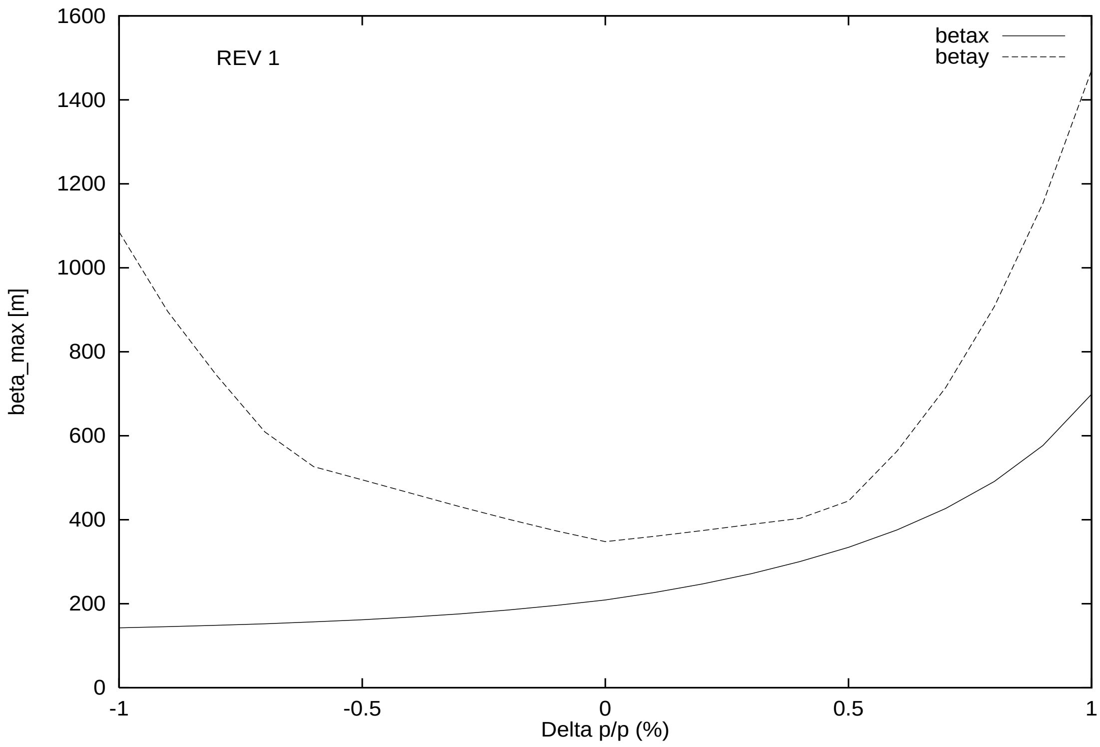

Figure 31: β_{max} in the complete ring vs δ for the REV 1 lattice

In this REV 1 lattice, the horizontal beta functions in the IRs are higher thus increasing the horizontal chromaticity compared to the REV 0 lattice so that the strengths of the sextupoles next to the horizontally focusing quadrupoles increased. This increases $dQ_x/d\epsilon_x$ in this lattice (as seen in Table 12) compared to the other lattices. The chromaticity correction for this lattice was done by minimizing both the second and third order chromaticities using HARMON in order to reduce the tune variation. The residual chromatic aberrations are still stronger in the horizontal plane compared to the previous lattices. Figure 29 shows that the tune changes lie in the range -0.01 $< \Delta Q_x <$ 0.025 over the full momentum range. Conversely, the geometric and chromatic aberrations in the vertical plane are much improved compared to the previous lattices. Figure 29 shows that -0.003 $< \Delta Q_y <$ 0.0015 over the momentum range. It should also be remembered that the nonlinear detunings are strong functions of the tune and changing the global tune with the arc quadrupoles can change these nonlinear parameters significantly. The optimal tune will be found by tracking and looking for the best dynamic aperture.

6.3.3 Dynamic Aperture without errors

We use two tracking programs to find the dynamic aperture. They are

- SIXTRACK - for fast, symplectic tracking to find the optimal tunes.
- MAD - slower tracking with the inclusion of radiation damping and quantum excitation at the optimal tunes.

Symplectic Tracking

Particles are tracked through the the linear and nonlinear elements in a lattice using the program SIXTRACK [5]. Symplecticity in all three planes is maintained. Typically pairs of particles are tracked with the particles in a pair having a very small difference in their initial amplitudes. The normalized distance between each pair is examined for signs of unstable growth. When the distance between any pair grows suddenly over a few turns by an order of magnitude or more, that is a sign of a positive Lyapunov exponent implying exponential instability. These particles may still stay within the beam-pipe for many many turns without being lost but the idea here is to identify the dynamic aperture as the region where there is a "sensitive dependence on initial conditions" and chaotic motion begins. Outside the dynamic aperture particles get lost fairly quickly. Use of the Lyapunov exponent to determine the dynamic aperture usually results in a conservative estimate compared to other methods [7]. In addition, this program also calculates the Fourier spectrum of the particles and the smear (defined as the variation of the linear Courant-Snyder invariant). Chaotic motion is also revealed in the spectrum with the presence of many lines and a typically "noisy" appearance. In our simulations, there is usually a good correspondence between the chaotic boundary as indicated by the Lyapunov analysis and that indicated by the spectrum. The smear is useful as a quick quide to the nonlinearity of particle motion. Smaller the growth of the smear with amplitude, better is the linearity of the lattice.

Typically 32 particles are tracked in pairs, with members of a pair differing in horizontal amplitude by 8×10^{-8}mm. For the initial tracking runs a tune scan is done to determine the optimal tunes where the dynamic aperture is largest. The initial vertical amplitude is calculated from the horizontal amplitude assuming an emittance coupling ratio of 10%. They are tracked for 1024 turns which is larger than the damping time of about 613 turns. On longer time scales we expect that the effect of the nonlinearities will be reduced by the synchrotron radiation damping. Hence most particle losses due to the instability of single particles should occur within a few damping times. Synchrotron oscillations are modelled in SIXTRACK by the inclusion of a single RF cavity. This is adequate when damping effects are not included. The tune of the lattice is varied by changing the strengths of the quadrupoles in the four arcs. This introduces a small beta-beat around the ring which should not affect the stability significantly. Tunes are chosen to avoid the major resonances of order less than 10, specially the 3rd and 4th integer resonances. Since the detuning with amplitude is stronger in the vertical plane for all lattices studied, some care was taken to keep the vertical tune further from a resonance line. In the tracking runs reported in this section, no errors - either of alignment, field or multipolar - were included in the lattice. The only nonlinearities were those of the chromaticity correcting sextupoles. Particle coordinates in all three planes are recorded and postprocessed. The smallest amplitude at which there is a sharp increase in the normalized distance between the members of a pair is taken to be the "dynamic aperture".

Dynamic apertures were determined for the lattices mentioned in the previous section for a range of tunes. This was used to first select the appropriate phase advance per cell and then to check if the stronger sextupoles needed to correct the larger chromaticity of the lattice due to the stronger focusing in the interaction regions still lead to an acceptable dynamic aperture.

Figure 32 shows the dynamic aperture at a range of tunes for the lattice with phase advances of 90 degrees in each plane (the lattice labelled I in table 11). The maximum dynamic aperture obtained with lattice I is about 15σ which is barely sufficient considering that errors and multipolar fields will reduce this value significantly. Consequently, the phase advance in the vertical plane was dropped to 60 degrees with the expectation that the lower chromaticity would lower the sextupole strengths and thereby improve the dynamic aperture.

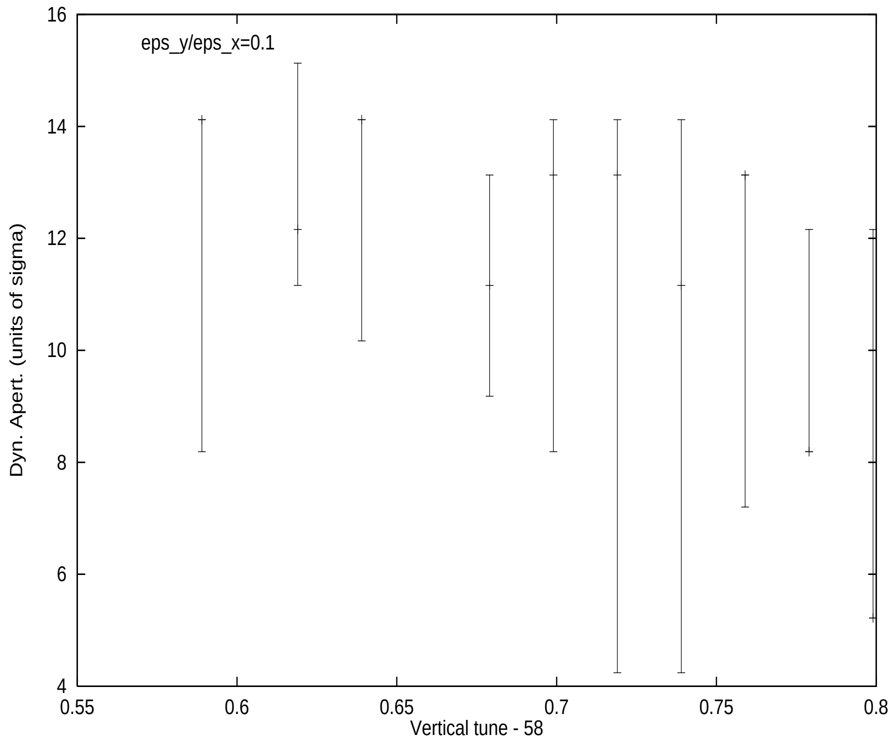

Figure 32: Dynamic aperture (in units of the rms beam size) as a function of the fractional vertical tune for the lattice with 90 degrees phase advance in both planes per cell in the arcs (lattice I). At each vertical tune, the dynamic aperture was calculated over a range of horizontal tunes. Each bar represents the minimum and maximum aperture obtained at that vertical tune.

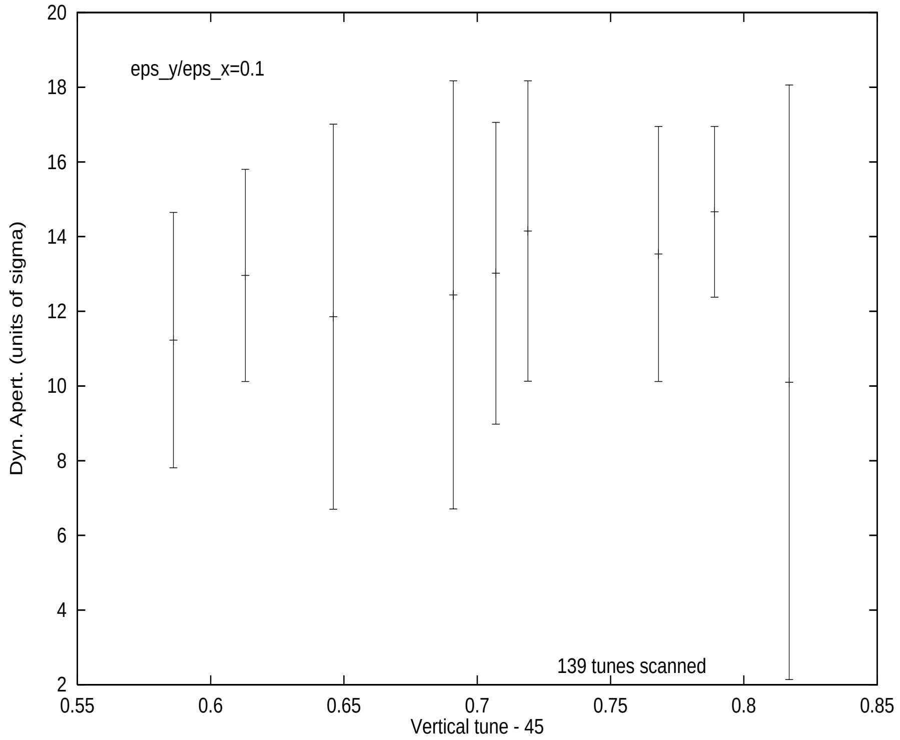

Figure 33: Dynamic aperture of the II (REV 0) lattice with phase advances of (90,60) degrees in the FODO cells. Similar remarks apply as for Figure 32

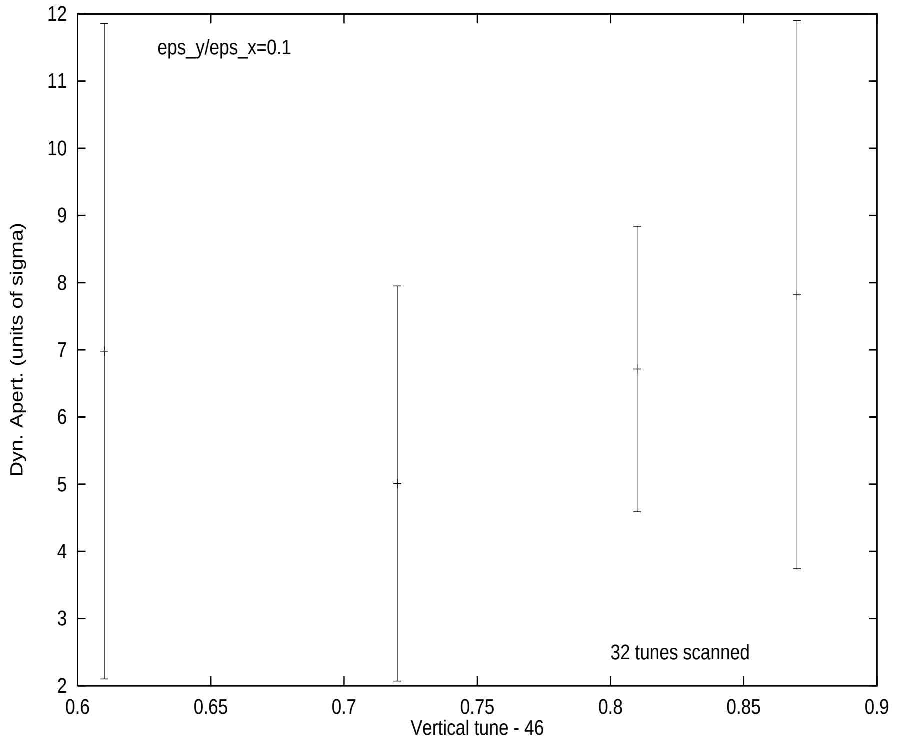

Figure 34: Dynamic aperture of lattice III with phase advances of (86.4,60) degrees in the FODO cells. Similar remarks apply as for Figure 32

With the vertical phase advance set to 60 degrees, the dynamic aperture of the lattices with 90 degrees and 86.4 degrees phase advance in the horizontal plane (II and III respectively) was determined. The numbers of sextupole families, phase advances between them and their strengths are quite different in the two lattices and that affects the dynamic aperture. Figures 33 and 34 show the dynamic aperture over a range of tunes. Lattice II (REV 0) has a maximum dynamic aperture of 18σ at several tunes. Lattice III has a significantly worse dynamic aperture with only a maximum of 12σ at the best tunes. This leads to the clear choice of (90,60) degrees as the phase advance per plane in the arc FODO cells.

Dynamic aperture of REV2

The chromaticity and the sextupole strength are considerably reduced in the Rev2 lattice in the vertical plane due to stronger focusing inside the detector. The horizontal chromaticity increases slightly, however. The reduction of the average chromaticity is expected to result in larger values of the dynamic aperture. Tracking calculations for the Rev2 lattice are in progress. Results are not available at this point.

6.3.4 Tracking with damping and quantum excitation

The emission of photons changes the electron orbit and can be usefully described as the sum of two effects: an average loss of energy over the orbit and a fluctuating energy loss about this average along the orbit. The first, also called radiation damping, helps to damp the electron orbit in all three planes towards the origin while the second, called quantum excitation, leads to a diffusive growth in the orbit. The balance between these two effects leads to the equilibrium emittance. Two dimensionless parameters can be used to characterize the strength of the radiation damping and quantum excitation: τ_x/T_0 the horizontal damping time in numbers of turns and Q_γ the ratio of the variance of the total photon energy emitted per turn to the square of the beam energy [8]. Smaller τ_x/T_0 implies that the effects of damping are more significant. Q_γ is given by

$$Q_\gamma = \frac{\langle N_\gamma \rangle \langle u^2 \rangle}{E^2} = \frac{55\pi}{36} \frac{\alpha_f (\hbar c)^2}{(m_0 c^2)^2} \frac{\gamma^5}{|\rho_0|^2} \tag{25}$$

where we have used the fact that the average number of photons emitted per turn is

$$\langle N_\gamma \rangle = \frac{5\pi}{\sqrt{3}} \alpha_f \gamma \ . \tag{26}$$

$\alpha_f = 1/137.036$ is the fine structure constant. The variance of the photon energy distribution is

$$\langle u^2 \rangle = \frac{11}{27} u_c^2 = \frac{11}{27} \left[\frac{3}{2} \frac{\hbar c \gamma^3}{|\rho_0|} \right]^2 \tag{27}$$

The average energy loss per turn is

$$U_\gamma = \frac{2}{3} r_e m_0 c^2 \gamma^4 \oint \frac{ds}{\rho^2} \ . \tag{28}$$

To estimate the strength of these effects for HERA relative to another high energy electron machine, we compare these parameters with those for LEP [9] in Table 13. We see that the effect of damping is nearly the same for the REV 1 design of HERA and LEP 1 while the quantum effects in HERA REV 1 are somewhat stronger than in LEP 1. Both of these effects are considerably stronger in LEP 2.

In the past radiation has usually been neglected when the dynamic aperture of electrons (or positrons) has been found by tracking. This has been justified by the belief that damping should help stabilize the motion and that would lead to a greater dynamic aperture. Jowett [8] has pointed out that the effects of radiation cannot be ignored at high energies. Since the energy of a particle on an orbit decreases between RF cavities and rises sharply at the cavities,

	HERA-e (REV 1)	LEP 1	LEP 2
Beam Energy E (GeV)	27.5	45.6	90.0
Radiation Loss per turn U_γ (MeV)	91	125	1890
Relative Energy Loss U_γ/E (%)	0.33	0.27	2.1
Damping time τ_x/T_0 (turns)	613	692	90
Quantum Excitation Q_γ (times 10^9)	6.4	2.8	79

Table 13: Comparison of damping and quantum excitation parameters for HERA-e and LEP 1 and LEP 2. The data for LEP are taken from [9].

the relative energy deviation $\delta_0(s)$ has a **sawtooth shape** along the orbit. The closed orbit which is six dimensional periodic solution of the equations of motion includes this behaviour of $\delta_0(s)$. The stable phase angle in synchrotron phase space is one component of the closed orbit and would be calculated incorrectly if the correct closed orbit were not found. With the wrong closed orbit (found by ignoring radiation) the fields seen by the particle and the calculated tunes would also be wrong. These might lead to an optimistic estimate of the dynamic aperture by ignoring e.g. the effects of synchro-betatron resonances excited by this additional energy variation. At LEP 1, these effects are thought to be not of great significance but at LEP 2 they are expected to be important. One hopes that at the energy and parameters of HERA-e, these effects are also not significant but it remains to be checked by tracking. This will be done in a future study.

An additional potentially unstable effect of radiation is the coupling of the transverse to the longitudinal dynamics [8]. Particles with large betatron amplitudes in quadrupoles lose additional energy generating **quadrupole synchrotron radiation**. This radiation is significant in the high beta quadrupoles in the interaction regions. Consequently the stable phase angle $\phi_s \simeq \sin^{-1}[U_{loss}/eV_{RF}]$ will change due to the extra loss of energy. The synchrotron oscillations will be about a shifted stable fixed point and it may happen that even particles with small energy deviation but large transverse amplitudes will make excursions outside the RF bucket and be lost. The magnitude of the shift in the phase angle can be estimated as

$$\begin{aligned} \Delta\phi_s &= \sin^{-1}\left[\frac{U_{dipoles}+U_{quad}}{eV_{RF}}\right] - \sin^{-1}\left[\frac{U_{dipoles}}{eV_{RF}}\right] \\ &\simeq \tan\phi_{s0}\left[\frac{I_{6x}A_x + I_{6y}A_y}{I_2}\right] \end{aligned} \tag{29}$$

where A_x, A_y are the horizontal, vertical actions respectively defined by the maximum transverse amplitudes

$$x_{max} = \sqrt{2\beta_x A_x}, \qquad y_{max} = \sqrt{2\beta_y A_y}\ . \tag{30}$$

I_2, I_{6x}, I_{6y} are the synchrotron radiation integrals

$$I_2 = \oint \frac{ds}{\rho^2} \tag{31}$$

$$I_{6x} = \oint K_x^2\beta_x ds, \qquad I_{6y} = \oint K_y^2\beta_y ds\ . \tag{32}$$

Since the design upgrade has increased the vertical β peak in the interaction region by more than a factor of two compared to the current design (see Table 11) we can expect that the effects

	CURRENT LATTICE	REV 1
I_2	1.08×10^{-2}	1.13×10^{-2}
I_{6x}	2.06×10^{2}	2.75×10^{2}
I_{6y}	1.80×10^{2}	3.80×10^{2}
$\Delta\phi_s$	0.83 mrad	1.35 mrad

Table 14: Synchrotron radiation integrals and the shift in stable phase angle ϕ_s at actions $2A_x = 2A_y = 22$ nm calculated for the current design lattice and the upgrade lattice REV 1

Error	Effect
Dipole Field Error Quadrupole alignment error (transverse)	Orbit Error
Quadrupole Field Error Sextupole alignment error	Change in the tune, beta beat, dispersion beat Small orbit error (from sextupole misalignment)
Roll misalignment in dipoles	Vertical orbit error
Roll misalignment in quadrupoles	Transverse coupling
Multipole field errors in dipoles, quadrupoles	Nonlinear fields on beam

Table 15: Various sources of errors and their effects on the beam

of quadrupole radiation will be more significant in the REV 1 design. In Table 14 we compare the synchrotron radiation integrals for the current and REV 1 designs. We also calculate the shift in the stable phase angle at actions $2A_x = 2A_y = 22$nm, the equilibrium emittance of REV 1. The nominal stable phase angle ϕ_{s0} in the absence of quadrupole radiation is 46.7 degrees. As expected I_{6y} is more than twice as large in the REV 1 design compared to the current design leading to a shift in the stable phase angle almost twice as large. The effect of this shift on the dynamic aperture will be determined by future tracking studies.

6.3.5 Dynamic Aperture with Errors

The different errors which inevitably exist in the magnets - both in their fields and alignments - enhance the unstable motion of particles and reduce the dynamic aperture. Table 15 shows the different kind of common errors and their effects on the dynamics.

Orbit errors change the trajectory of particles through the nonlinear elements which also causes a detuning. Typically orbit errors alone can reduce the dynamic aperture by a significant fraction. The dynamic aperture in the presence of the errors mentioned above will be studied once the lattice (either REV1 or REV2) has been chosen as the working lattice.

References

[1] H. Wiedemann, Nucl. Instr. Methods, **172**, 33 (1980)

[2] T. Sen and M. Syphers, Proc. 1993 IEEE Part. Acc. Conf, pg 140 (1993)

[3] K.L. Brown, IEEE Trans. Nuc. Sci. **NS-26**, 3490 (1979)

[4] R. Brinkmann and F. Willeke, DESY 87-037 (1987)

[5] F. Schmidt, CERN/SL/94-56(AP)

[6] H. Grote and F.C. Iselin, CERN/SL/90-13(AP)

[7] F. Schmidt, F. Willeke, F. Zimmerman, DESY HERA 91-07 (1991)

[8] J. Jowett, Proc. 4th Workshop on LEP Performance, CERN SL/94-06, 47 (1994)

[9] F. Barbarin et al., Proc. EPAC 1994, CERN SL/94-57(AP)

6.4 Solenoid Compensation with Skew Quadrupoles

The coupling of the betatron oscillations generated by a detector solenoid can be compensated most effectively by a second alternatively powered solenoid which is situated closely to the detector solenoid. Thus the rest of the ring is not affected by the coupling action of the two solenoids.

By this principle the coupling of the detector solenoids of ZEUS and H1 are compensated. In the design of the new interaction region for the luminosity upgrade however the compensating solenoids are removed in order to provide additional space so that the low beta quadrupoles can be placed as close as possible to the interaction point. This means that the coupling of the detector solenoids has to be compensated somewhere else in the ring. In the case of the HERA-proton ring this is done by a pair of skew quadrupoles in the west straight section. However, this kind of global compensation of coupling is not sufficient for the HERA-electron ring since coupling interfers with the conditions for having a polarized beam. Therefore this section considers a scheme where the low beta quadrupoles at each side of the detector solenoid are rotated slightly in order to provide a local compensation of coupling.

The coupled betatron oscillations have two eigenmodes: the sum resonance which corresponds to the π-mode of two coupled oscillators and the difference resonance representing the $\frac{\pi}{2}$-mode. Firstly, the coupling strengths generated by the detector solenoids are calculated for the two eigenmodes, respectively. The necessary rotation angles of the low beta quadrupoles are evaluated for the compensation of coupling in the mode of difference resonance only since the tunes in the electron ring are close to the values which fulfill this resonance condition. For this the coupling strength generated from the right and left part of the detector solenoid with respect to the interaction point is considered independently. The low beta quadrupoles on the right and left hand side of the interaction point then are rotated to compensate the coupling from the right and left part of the solenoid respectively.
The coupling strength generated by the inner part of the detector solenoid is described by the integral:

$$\kappa_{sc} = \frac{1}{4\pi} \int_{ip}^{L_s} ds \quad M\sqrt{\beta_x\beta_y}\left[\frac{1}{2}\left(\frac{\alpha_x - \alpha_y}{\beta_x - \beta_y}\right) - \frac{i}{2}\left(\frac{1}{\beta_x} - \frac{n}{\beta_y}\right)\right] \cdot \quad e^{i(\phi_x + n\phi_y)}, \tag{33}$$

whereas the contribution of the solenoid fringe field to the coupling strength is given by:

$$\kappa_{sf} = \frac{1}{4\pi} \quad M\frac{1}{2}\sqrt{\beta_x\beta_y} \cdot \quad e^{i(\phi_x + n\phi_y)} \quad . \tag{34}$$

Here

$$M = \frac{ec}{E_0} B_s \tag{35}$$

is the fieldstrength of the solenoid and n distinguishes between the two resonance modes:

$$n = +1 : \quad sum\ resonance$$
$$n = -1 : \quad difference\ res.$$

The following numbers are derived from equations 33 and 34 by assuming a magnetic field of 1.4 T in the ZEUS solenoid and 1.5 T in the solenoid of H1. Further it is assumed that the

ZEUS solenoid is arranged symmetricaly around the interaction point with a total extension of 2.4 m whereas the solenoid of H1 is extended by 3 m to the left and by 4 m to the right side with respect to the IP. First estimates indicate that the low-β quadrupoles QI and QJ will have to be rotated by $2mrad$. In addition, it is desirable to have small tunable skew-quadrupoles installed in the lattice. These magnets will be specified according to the needs of spin matching. This has not yet been completed.